Non symmetrical sterically challenged phenanthroline ligands and their homoleptic copper(I) complexes with improved excited state properties

Lea Gimeno, Errol Blart, Jean-Noël Rebilly, Marina Coupeau, Magali Allain, Thierry Roisnel, Alexis Quarré de Verneuil, Christophe Gourlaouen, Chantal Daniel, Yann Pellegrin

10.1002/chem.202001209

WILEY-VCH

FULL PAPER

Non symmetrical sterically challenged phenanthroline ligands and their homoleptic copper(I) complexes with improved excited state properties

Lea Gimeno,[a] Errol Blart,[a] Jean-Noël Rebilly,[b],* Marina Coupeau,[a] Magali Allain,[c] Thierry Roisnel,[d] Alexis Quarré de Verneuil,[a] Christophe Gourlaouen,[e],* Chantal Daniel,[e] and Yann Pellegrin[a],*

Abstract: A strategy is presented to improve the excited state reactivity of homoleptic copper-bis(diimine) complexes CuL_2^+ by increasing the steric bulk around Cu(I) while preserving their stability. Substituting the phenanthroline on position 2 by a phenyl group allows the implementation of stabilizing intramolecular π stacking within the copper complex, while tethering a branched alkyl chain on position 9 provides enough steric bulk to rise the excited state energy E^{00}. Two novel complexes are thus studied and compared to symmetrical models. The impact of breaking the symmetry of phenanthroline ligands on the photophysical properties of the complexes is analyzed and rationalized thanks to a combined theoretical and experimental study. The importance of fine-tuning the steric bulk of the N-N chelate in order to stabilize the coordination sphere is demonstrated. Importantly, the excited state reactivity of the newly developed complexes is improved as demonstrated in the frame of a reductive quenching step, evidencing the relevance of our strategy.

Introduction

Copper(I) complexes of the general formula $[Cu(NN)_2]^+$ where NN is a diimine ligand bearing bulky substituents in α of the nitrogen atoms are appealing luminophores in the frame of photosensitive coordination compounds.[1] Indeed, they exhibit photo-physical properties which are similar to those of benchmark $[Ru(bpy)_3]^{2+}$.[1a, 1c, 2]. In particular they are luminescent upon excitation in the Metal to Ligand Charge Transfer (MLCT), provided that encumbering groups are appended in α of the chelating nitrogen atoms. During excitation (equation 1), the metal formally shifts from Cu(I) (favored tetrahedral geometry) to Cu(II) (favored square-planar geometry).

$$[Cu^{I}L_2]^+ + hv \rightarrow [Cu^{II}L^{\bullet-}L]^+ \text{ (equation 1)}$$

The coordination sphere relaxes in the $[Cu^{II}L^{\bullet-}L]^+$ excited state by flattening which opens several channels for efficient and counter-productive extinction of the luminescence.[3] Consequently, the excited state energy levels dynamically shift to lower energy on a typical 10-100 ps time scale, favoring non radiative de-excitation of the excited states (gap law). Besides, flattening of the transient copper(II) ion opens a fifth binding site for a ligand (e.g. a solvent molecule) leading again to the very fast so-called "exciplex quenching" of the excited state.[4] Encumbering groups limit the extent of the photo-induced flattening, thus promoting the luminescence of copper(I) complexes. Consequently considerable efforts have been made to improve the luminescence of copper(I) complexes by increasing the steric bulk around Cu(I).[5] The latter can be brought by either aliphatic (type I complexes, figure 1) or aromatic (type-II complexes) substituents. Impressive luminescence quantum yields have been obtained with type-I complexes by Castellano and co-workers with $[Cu(dipp)_2]^+$, $[Cu(tmdsbp)_2]^+$,[5b, c, 6] or Burstyn and co-workers with $[Cu(dtbp)_2]^+$[5a, 7] (where dipp stands for 2,9-diisopropyl-1,10-phenanthroline, tmdsbp stands for 2,9-di-secbutyl-3,4,7,8-tetramethyl-1,10-phenanthroline and dtbp for 2,9-di*tert*-butyl-1,10-phenanthroline). Remarkably, $[Cu(dtbp)_2]^+$ featured even better photophysical parameters than $[Ru(bpy)_3]^{2+}$ (luminescence lifetime of 3.26 µs vs. ca. 1 µs respectively) but the stability of the coordination scaffold was sacrificed. Indeed, the copper(I) complex is so sterically burdened that it quantitatively decomposes in presence of a weak ligand like acetonitrile.[5a]
Type-II $[Cu(dpp)_2]^+$ reported by Sauvage and co-workers (and parent complexes) also proved very luminescent[8] even at room temperature in presence of strongly coordinating species (e.g. water or acetonitrile): the complex is rigidified and shielded by the phenyl groups, π-stacked to the vicinal phen ligand.[9] But the latter interactions substantially distort the coordination cage entailing a decrease of the singlet state energy E^{00}.[10] This in turn impact negatively the reactivity of the excited state, by virtue of the Rehm and Weller equation.

[a] Lea Gimeno, Marina Coupeau, Alexis Quarre de Verneuil, Dr. Errol Blart, Dr. Yann Pellegrin
Université de Nantes, CNRS
CEISAM UMR6230
F-44000 Nantes, France
E-mail: yann.pellegrin@univ-nantes.fr
[b] Dr. Jean-Noël Rebilly
ICMMO, UMR 8182
Université Paris Sud, Université Paris Saclay
Orsay 91405 cedex, France
[c] Magali Allain
Laboratoire MOLTECH-Anjou, UMR CNRS 6200
Univ Angers, SFR MATRIX
2 Bd Lavoisier, 49045 Angers Cedex, France
[d] Thierry Roisnel
Université de Rennes CNRS
Institut des Sciences Chimiques de Rennes
UMR6226
F-35000 Rennes, France
[e] Dr. Christophe Gourlaouen, Pr. Chantal Daniel
Laboratoire de Chimie Quantique Institut de Chimie UMR 7177
CNRS-Université de Strasbourg, 4, Rue Blaise Pascal CS 90032, F-67081 Strasbourg Cedex, France

Supporting information for this article is given via a link at the end of the document.

10.1002/chem.202001209
WILEY-VCH

FULL PAPER

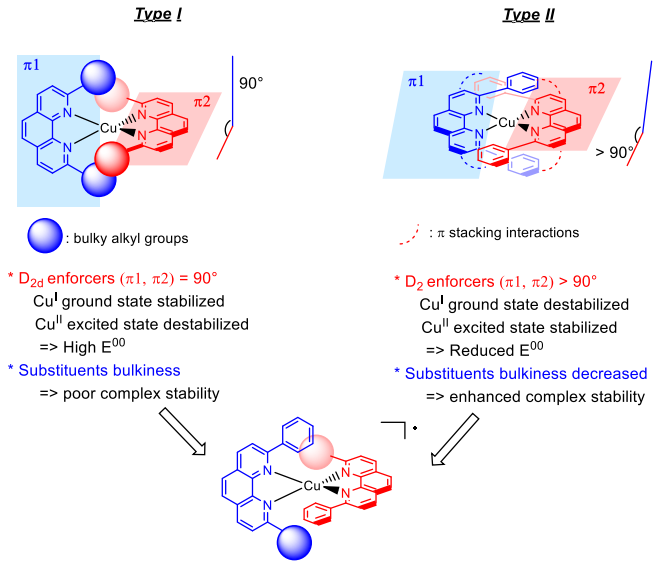

Figure 1. Illustration of the strategy developed in this contribution

Summarily, very bulky aliphatic groups like *tert*-butyl in α of the nitrogen atoms endow the corresponding copper(I) complex with long lived, intense luminescence and high E^{00} while aromatic groups confer improved stability to the coordination cage, maintain significant luminescence lifetime and quantum yield, but lead to a smaller E^{00}.

In this contribution, we explore a strategy to implement intramolecular π-stacking while maintaining the tetrahedral geometry to secure high E^{00}. Our approach is based on non-symmetrical phen ligands substituted by one phenyl group on one side and one bulky branched alkyl chain (isopropyl: ligand **L1**; or tert-butyl: ligand **L2**) on the other.

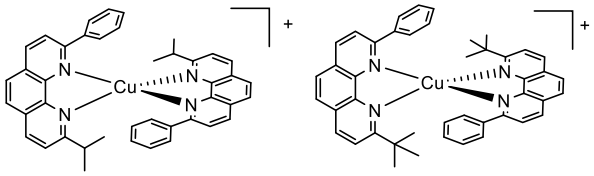

$[Cu(\mathbf{L1})_2]^+$, **C1** $[Cu(\mathbf{L2})_2]^+$, **C2**

Figure 2. Structures of the complexes investigated therein.

The resulting homoleptic copper complexes, **C1** and **C2** (figure 2) are a "fusion" of $[Cu(dpp)_2]^+$ with $[Cu(dipp)_2]^+$ and $[Cu(dtbp)_2]^+$, respectively, and would benefit from the stabilizing intramolecular phenyl-phenanthroline π-stacking interactions while the steric bulk provided by the alkyl chains (isopropyl or *tert*-butyl) contribute reaching a high E^{00}. We describe the synthesis and full optical and electrochemical characterization of **C1** and **C2**. The structural and optical properties of the two complexes have been analyzed by means of density functional theory (DFT). Our goals are 1) to find out if intramolecular π-stacking can take place within the complex despite the presence of bulky ramified chain on the same ligand; 2) to assess the stability of the corresponding coordination scaffold vs. the steric strain; 3) to observe if the energy of the excited state can be increased and how it impacts the reactivity of the excited state.

Results and Discussion

The synthesis of ligands **L1** and **L2** was performed in two steps, by addition of the corresponding organolithium reagents on anhydrous phenanthroline and re-aromatization with MnO_2 (scheme 1). Other synthetic pathways have been envisioned (for instance, an improved Povarov approach has been successfully developed to synthesize ligand **L1**)[11] but the organolithium route proved to be more efficient in our hands. The synthesis of the three corresponding copper(I) complexes proceeded smoothly, by mixing two equivalents of ligand with one equivalent of tetrakis(acetonitrile)copper hexafluorophosphate in degassed dichloromethane.

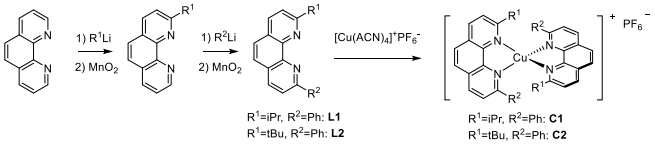

Scheme 1. Synthesis of ligands **L1**, **L2** and of complexes **C1** and **C2**.

The bright red powders were characterized by ^{1}H-NMR and mass spectrometry, all the analyses confirm the proposed structures. Monocrystals of ligand **L2** and complex **C2** were obtained by slow diffusion of hexane in a dichloromethane solution of the corresponding molecule, and their structures could be resolved by X-ray diffraction. Relevant parameters are reported in table ST1 (supporting information). The structure of **L2** (figure S1, supporting information) reveals as expected a very sterically strained environment around chelating nitrogen atoms. The phenyl group tethered to C_{12} is slightly twisted with respect to the phenanthroline plane (twist angle = ca. 25.3°), due to repulsion between protons H_{11} and H_{14} and possibly crystal packing forces. The structure of complex **C2** is given in figure 3 (ORTEP view available in figure S2). Basically, the CuN_4 coordination sphere is a flattened tetrahedron; the τ_4 parameter for **C2** is almost exactly the average between $[Cu(dpp)_2]^+$ and $[Cu(dtbp)_2]^+$ (figure S6). However **C2**'s structure is closer to a type-I complex than a type-II, despite the presence of the aryl group in α of the nitrogen atom.

Figure 3. Two views for the structure of complex **C2**.

10.1002/chem.202001209

Rather unfavorable angles between phenyl groups C and E and phenanthroline B and A respectively (aromatic cycles and relevant atom nomenclature is given in figure S3) are measured (more than 30° vs. ca. 10° in the case of $Cu(dpp)_2^+$)[9a] and the distance between the aromatic cores is larger (more than 4 Å) meaning that the extent of intramolecular π stacking is likely smaller than for $[Cu(dpp)_2]^+$ in the crystal phase. A relevant way to quantitatively estimate how distorted from the ideal D_{2d} symmetry copper complexes are, consists in calculating θ_x, θ_y and θ_z angles, respectively the rocking, waggling and flattening angles (see figures S4-6 in supporting information for an illustration of those angles).[12] For a perfectly tetrahedral geometry, $\theta_x = \theta_y = \theta_z = 90°$; this is roughly the case for $[Cu(dtbp)_2]^+$ (table ST1, figure S6). For $[Cu(dpp)_2]^+$, the intramolecular stacking interactions lead to a strongly distorted structure ($\theta_x = 104.6$, $\theta_y = 69.8$, $\theta_z = 100.2$). On the other hand, **C2**'s structure is not perfectly tetrahedral since θ_z is significantly different from 90° revealing the coordination sphere is substantially flattened in the ground state, but to a lesser extent than $[Cu(dpp)_2]^+$, as exemplified by θ_x and θ_y values which are close to 90°. All in all, the $\theta_{x,y,z}$ parameters of **C2** are closer to those of plain $[Cu(dmp)_2]^+$.[12] This means that the steric bulk imposed by the *tert*-butyl group limits the development of intramolecular π stacking within the complex in the crystal phase. Nevertheless, let us pinpoint that the phenyl group is more twisted with respect to the phenanthroline plane onto which it is tethered (C on A, E on B) passing from the free ligand to the complex. This could be a proof that some interaction between C and B (and E and A) is taking place. CH-π interactions are possible in this frame (Figure S7). Accordingly, crystal packing could account for this observation too. Importantly, no significant intermolecular interaction is observed in the structure. In solution, it is interesting to notice that the chemical shifts assigned to hydrogen atoms on the phenyl groups tethered on phenanthroline are step wisely shielded when passing from $[Cu(dpp)_2]^+$ to **C1** then **C2** indicating that the orientation of the bulky aromatic groups is different (table ST2), resulting from a mixture of steric constraints, π-stacking and possible CH-π interactions.

UV-Vis absorption

UV-Vis spectra were recorded for **C1** and **C2** in dichloromethane solutions (figure 4) and experimental data are gathered in table 1. Both complexes exhibit the same absorption features, namely intense ligand centered π-π* transitions below 370 nm and a broad band assigned to the MLCT spanning between 400 and 500 nm and responsible for the bright orange color of all complexes.

A shoulder is monitored above 500 nm for all complexes but is more prominent for **C1** than **C2**. For symmetry reasons, the $S_0 \rightarrow S_1$ transition is forbidden in the case of tetrahedral copper(I) complexes and the MLCT peaking at ca. 460 nm is thus a $S_0 \rightarrow S_n$ ($n > 1$) transition. When the geometry moves away from tetrahedral, the $S_0 \rightarrow S_1$ transition becomes partially allowed.

The intensity of the S_0 to S_1 transition thus allows to estimate the degree of flattening in a copper(I) complex in its ground state.[5h, 13] $[Cu(dpp)_2]^+$ shows a rather significant S_0 to S_1 transition in the shape of a broad shoulder,[14] whereas no such spectral feature can be detected for $[Cu(dtbp)_2]^+$ (virtually perfectly tetrahedral). This indicates a significant symmetry descent from D_{2d} to D_2, in line with the favorable π-stacking interactions between the phenyl and the adjacent phenanthroline.[15]

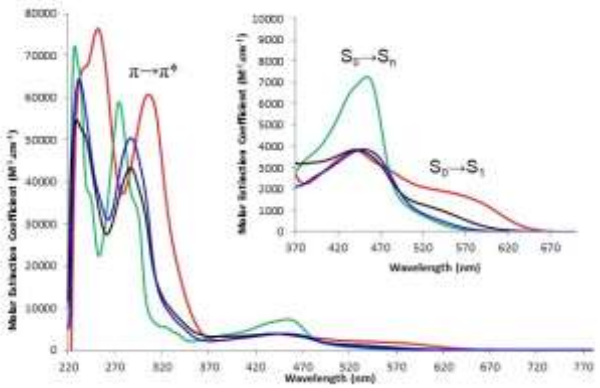

Figure 4. Electronic absorption spectra for complexes **C1** (black trace), **C2** (blue trace), $[Cu(dipp)_2]^+$ (green trace) and $[Cu(dpp)_2]^+$ (red trace) recorded in dichloromethane at room temperature. Average concentrations 0.05 mM.

All other $[Cu(NN)_2]^+$ complexes are located in between those two extremes, featuring shoulders of variable intensity at the stem of the MLCT. In our case, one can learn from normalized absorption spectra (figure S8) that the structure of **C1** is substantially more flattened in the ground state than **C2** or benchmark $[Cu(dipp)_2]^+$. This proves that the phenyl substituent in ligand **L1** is capable of intramolecular π-stacking with the vicinal phenanthroline. On the other hand, the *tert*-butyl group in **L2** imposes a stronger steric bulk which restrains the flattening in **C2** and limits the possibility of π-π interactions. This corroborates the observations made on the solid state where the 30° angle and the distance between phenyl C and phenanthroline B (figure S3) are more in line with CH-π interactions (figure 3).

Electrochemistry

The electrochemical behavior of complexes **C1** and **C2** was explored by cyclic voltammetry in dichloromethane and dimethylformamide (DMF) solutions, in presence of tetrabutylammonium hexafluorophosphate as supporting electrolyte. The voltammograms are given in figures S9 and S10; and related data are reported in table 1. One mono-electronic, pseudo-reversible oxidation wave was monitored and assigned to the Cu^{II}/Cu^{I} couple for both complexes ($E_1 = 0.49$ and 0.55 V vs. ferrocenium/ferrocene redox couple (Fc^+/Fc) for **C1** and **C2** respectively). Generally speaking, **C1**, **C2** and $[Cu(dpp)_2]^+$ are oxidized at similar potentials, significantly less positive than $E_1(Cu(dipp)_2^+)$. Indeed, bulky substituents enforce a D_{2d} symmetry which stabilizes the copper(I) ion and induce a more anodic oxidation potential.[5d, 5h, 16] Phenyl substituents generate intramolecular π-stacking and entail a descent to D_2 symmetry and thus a shift of the oxidation potential to less positive values vs. $[Cu(dipp)_2]^+$.[5a] **C2** is undeniably more sterically burdened than **C1** because of the *tert*-butyl group, which translates into E_1(**C2**) > E_1(**C1**).

10.1002/chem.202001209

Table 1. UV-Vis and electrochemical data for complexes **C1**, **C2**, $[Cu(dpp)_2]^+$ and $[Cu(dipp)_2]^+$ in dichloromethane. All data recorded at room temperature. Electrochemical potential values reported vs. the Fc^+/Fc couple taken as internal standard.

Complexes	λ_{max}/nm	$\varepsilon_{\lambda max}$/L.mol^{-1}cm^{-1}	E_1 (ΔE)/V (mV)[a]	E_2 (ΔE)/V (mV)[b]
C1	443, 540	3990, 1000	0.49 (120)	-2.06 (130)
C2	450	3850	0.55 (110)	-2.08 (90)
$[Cu(dpp)_2]^+$	439, 550	3800, 1800	0.53 (80)	-2.07 (120)
$[Cu(dipp)_2]^+$	453	7260	0.65 (120)	-2.10 (75)

[a] Degassed dichloromethane solutions, sweep rate for electrochemical measurements = 100 mV.s^{-1}. [b] Degassed DMF solutions, sweep rate for electrochemical measurements = 1 V.s^{-1}. $E_1 = (E^{p,a}{}_1 + E^{p,c}{}_1)/2$, $E_2 = (E^{p,a}{}_2 + E^{p,c}{}_2)/2$; $\Delta E = E^{p,a}{}_1 - E^{p,c}{}_1$ or $E^{p,a}{}_2 - E^{p,c}{}_2$, where $E^{p,a}{}_1$, $E^{p,c}{}_1$, $E^{p,a}{}_2$ and $E^{p,c}{}_2$ are anodic and cathodic peak potentials for electrochemical processes 1 and 2, respectively.

Both **C1** and **C2** are expected to be less flattened than $[Cu(dpp)_2]^+$, but nevertheless, $E_1([Cu(dpp)_2]^+) > E_1$(**C1**). Rationalizing the order of their close oxidation potentials is made particularly difficult by the interplay of both steric and electronic effects.

No reduction wave was observed within the solvent electro-activity window of dichloromethane. In DMF however, a pseudo-reversible wave was monitored below -2 V vs. Fc^+/Fc as internal standard for all complexes and was assigned to the addition of an extra electron on one phenanthroline ligand. All potential values E_2 are very close to each other despite the differences between the electronic effects from branched alkyl chains (electron rich) and the aromatic groups (electron poor).

Excited state properties

Complexes were studied by steady state fluorescence and time-correlated single photon counting in degassed dichloromethane. All complexes are luminescent at room temperature in dichloromethane dilute solutions. Steady state emission spectra are given in figure 5, while decay traces are given in figures S11 and S12. Emission maximum wavelengths λ_{em}, luminescence quantum yields ϕ_{lum}, lifetimes τ and E^{00} values (energy difference between singlet excited state and the ground state in ground vibrational states, estimated by the tangent method)[5b] are reported in table 2.

Concerning model complexes $[Cu(dpp)_2]^+$ and $[Cu(dipp)_2]^+$, bulky isopropyl groups in the latter tend to favour D_{2d} ground state geometry and a stabilized environment for copper(I) affording short emission wavelength and large E^{00}. Conversely, intramolecular π-stacking in $[Cu(dpp)_2]^+$ entail the flattening of the coordination cage towards D_2 symmetry, destabilization of the copper(I) ion and thus longer emission wavelength and smaller E^{00}. All figures of merit for **C1** and **C2** are comprised between those of the model complexes. λ_{em} (**C1**) is red shifted compared to $\lambda_{em}([Cu(dipp)_2]^+)$ precisely because of the intramolecular π-stacking interaction entailing some significant distortion of the coordination sphere away from D_{2d}; conversely the steric bulk from the branched isopropyl chain tends to oppose to this ground state distortion, forcing **C1** in a less distorted geometry than $[Cu(dpp)_2]^+$, hence λ_{em} (**C1**) is blue shifted compared to $\lambda_{em}(Cu(dpp)_2^+)$ and E^{00} is larger. These results are comparable with those obtained by Miller et al. where dpp-like ligands were progressively encumbered with substituents, gradually limiting the π-stacking interaction within the corresponding complexes.[5h] **C2**'s emission wavelength is further blue-shifted due to the even greater steric strain brought by *tert*-butyl (compared to isopropyl), with similar λ_{em} and E^{00}. Conclusively, increasing the steric bulk with one ramified alkyl chain on one side of phenanthroline while keeping a phenyl group on the other allowed to increase E^{00} compared to $[Cu(dpp)_2]^+$ and maintain significant π-stacking interaction at least for the case of **C1**.

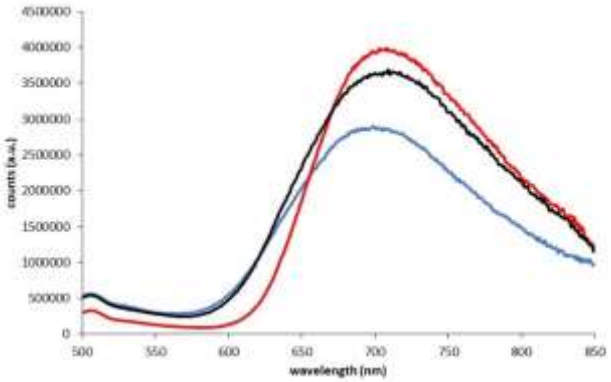

Figure 5. Emission spectra for complexes **C1** (black trace), **C2** (blue trace) and $Cu(dpp)_2^+$ (red trace) recorded in dilute dichloromethane solutions (ca. 0.05 mM) at room temperature.

C1 and **C2** exhibit similar emission quantum yields than model $[Cu(dpp)_2]^+$, but unexpectedly short lifetimes, especially for **C2** (table 2). As a matter of fact, the emission lifetimes for **C2** and simple $Cu(dmp)_2^+$ are comparable, although the latter is less sterically strained. In order to deepen the study, we extracted the radiative and non-radiative rate constants (respectively k_r and k_{nr}) from our experimental data (table 2). **C2** exhibits the second best k_r (behind $[Cu(dipp)_2]^+$), which can be assigned to its blue shifted absorption and emission bands compared to **C1** or $[Cu(dpp)_2]^+$, because k_r is proportional to the cube of the radiative energy gap.[5h, 17] The reason for the weak emission properties of **C2** are therefore not grounded in k_r. k_{nr} is however larger for **C1** and especially **C2**. A similar behavior was observed with the copper(I) complex $[Cu(MeMap)_2]^+$ (where MeMap is a non-symmetrical phenanthroline ligand bearing one anisyl and one methyl group in α of the chelating nitrogen atoms)[18] and seems related to the non-symmetrical nature of the ligands.

As reported in previous works, a phen ligand substituted by an aromatic and an aliphatic groups provides a very bulky environment on one side of the corresponding complex and at the same time a less bulky environment on the other.[19] This can be exacerbated in the excited state and interactions of the exposed copper(I) center with solvent molecules or counter-anions would thus be favored.

Table 2. Excited state parameters for complexes **C1**, **C2**, $Cu(dpp)_2^+$ and $Cu(dipp)_2^+$. Potentials are given vs. Fc^+/Fc.

complexes	λ_{em}/nm	ϕ_{lum}/%	τ/ns	E^{00}/eV	E_{ox}*/V	k_r / s^{-1}	k_{nr} / s^{-1}	k_{ACN} / $s^{-1}.M^{-1}$	k_{RQ} / $s^{-1}.M^{-1}$
C1	698	0.10	216	2.09	0.03	$4.63x10^3$	$4.63x10^6$	$1.09x10^9$	$1.8x10^9$
C2	678	0.08	92	2.11	0.03	$8.70x10^3$	$1.09x10^7$	-	$2.8x10^9$
$Cu(dpp)_2^+$	732	0.10	243	2.00	-0.07	$4.12x10^3$	$4.11x10^6$	$6.88x10^8$	$0.8x10^9$
$Cu(dipp)_2^+$	679	0.40	365	2.11	0.01	$1.10x10^4$	$2.73x10^6$	$9.16x10^8$	$3.1x10^9$

Such a process is particularly prominent with coordinating species (exciplex quenching) but has been monitored with non-coordinating molecules too.[20] Generally speaking, the solvent is known to have an influence on the ground and excited state properties of copper(I) complexes,[21] and this influence could be stronger when non-symmetrical ligands are coordinated to Cu(I) and lead to large k_{nr}. Tentatively, we recorded the luminescence decays of **C1**, **C2**, $[Cu(dpp)_2]^+$ and $[Cu(dipp)_2]^+$ in dichloromethane while progressively adding acetonitrile, well known to quench the emission of the copper complexes by exciplex formation, in order to appreciate how affected **C1** and **C2** are compared to classical $[Cu(dipp)_2]^+$ and $[Cu(dpp)_2]^+$. Following a Stern-Volmer analysis we could retrieve the quenching constants k_{ACN} (figure S13, table 2) of the emission by acetonitrile. The exciplex quenching is undeniably more efficient for **C1** than $[Cu(dipp)_2]^+$ or $[Cu(dpp)_2]^+$, the latter being as previously observed the most resilient.[8a] **C2** proved to be too unstable in presence of acetonitrile to allow recording spectra in the same conditions, but preliminary analysis of the data shows a very efficient emission quenching too. The enhanced exciplex quenching for **C1** and **C2** likely contributes to their particularly high k_{nr}.

Computational chemistry

Structures

The presence of phenyl moieties in the **C1** and **C2** complexes generates several $[Cu(dpp)_2]^+$-type conformers, the structures of which have been fully optimized at the DFT level. The structure of $[Cu(dipp)_2]^+$ complex belongs to the D_{2d} symmetry group. For $[Cu(dpp)_2]^+$, two conformers are possible, one of *D₂* symmetry and one of *S₄* symmetry (Figure 6). The *D₂* structure is significantly more stable than the S_4 one (ΔG = 2.3 kcal mol^{-1} computed at the DFT level) in accordance with experimental observations.[9a] The origin of the greater stability of the *D₂* structure can be attributed to π-stacking interactions as shown by the analysis of Non-Covalent Interactions (NCI) (figure 6). Whereas in the *D₂* structure, π-stacking is enhanced by the interaction between the phenyl groups of one ligand and the phenanthroline moiety of the second one, it is weakened in the *S₄* structure where the two moieties are less parallel. Furthermore, to ensure a greater parallelism between these moieties, the D_2 structure is already flattened in the ground state. **C1** and **C2** also exhibit conformers due to different orientations of the phenyl rings. In **C1**, the two computed structures have the same energy (ΔG = 0.0 kcal mol^{-1}). For **C2**, the structure issued from the X-ray data (figure 3) is slightly less stable than the conformer (ΔG = -0.6 kcal mol^{-1} computed at the DFT level, Figure 6). Such variations are the result of the competition between the stabilizing π-stacking interactions generated by the phenyl moieties and the steric congestion induced by the isopropyl and *tert*-butyl groups. In order to discuss the theoretical results in light of those two possible conformers, we will name *RX* the structures similar to what is pictured in Figure 3 (and calculated as presented in Figure 6, left side) and *conf* the second computed structure (calculated as presented in figure 6, right side) for $[Cu(dpp)_2]^+$, **C1** and **C2** complexes.

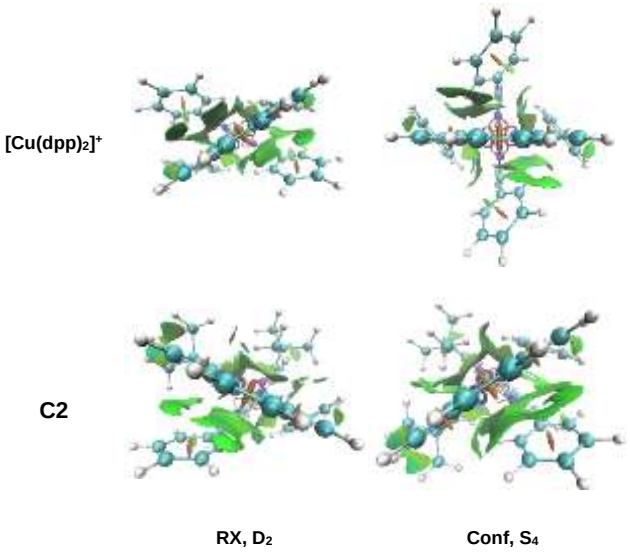

Figure 6. NCI analysis performed on the *RX* (top left) and *conf* (top right) structures of the $[Cu(dpp)_2]^+$ complex and on the *RX* (bottom left) and *conf* (bottom right) structures of **C2**. In green are the basins corresponding to Van der Waals forces and in red area of steric congestion. All the structures have been fully optimized in the electronic ground state with GAUSSIAN (see computational details).

Absorption

The absorption spectra were computed on the DFT/B3LYP optimized structures (Table 3) of $[Cu(dipp)_2]^+$, $[Cu(dpp)_2]^+$, **C1** and **C2** complexes and of their conformers (Figure 7). As observed experimentally, the visible domain is assigned to MLCT transitions and the UV-Visible domain to transitions localized on the ligands. The computed spectra of $[Cu(dipp)_2]^+$ is very similar to the experimental one with an intense band at 485 nm. Two singlet states are present at higher wavelength (505 and 522 nm) with no intensity for symmetry reasons. A shoulder is present at lower wavelength (433 nm).

The agreement between experimental (figure 3) and theoretical results (figure 7) is less good for the three other complexes in their *RX* structure. We retrieve the drop of the main $S_0 \rightarrow S_n$ band intensity and the appearance of smaller bands. For $[Cu(dpp)_2]^+$, the overall structure of the spectrum is well reproduced though being red shifted as compared to the experimental one. The main absorbing band is located at 454 nm. Four absorbing singlet

10.1002/chem.202001209

states are located at 549, 582, 584 and 628 nm generating the band between 570 to 650 nm.

Table 3. Geometric parameters of the ground state of $[Cu(dipp)_2]^+$, $[Cu(dpp)_2]^+$, **C1** and **C2** complexes and of their conformers. Distances are in Angstroms and angles in degrees. For each complex are given the relative stabilities (ΔE) between the *RX* and *conf* structures from ADF calculations.

State	$[Cu(dipp)_2]^+$	$[Cu(dpp)_2]^+$		**C1**		**C2**	
		RX	conf	RX	conf	RX	conf
$Cu\text{-}N_{1A}$	2.061	2.063	2.095	2.146	2.088	2.031	2.037
$Cu\text{-}N_{2A}$	2.061	2.063	2.095	2.024	2.058	2.180	2.162
$Cu\text{-}N_{1B}$	2.061	2.063	2.095	2.146	2.088	2.031	2.037
$Cu\text{-}N_{2B}$	2.061	2.063	2.095	2.024	2.058	2.180	2.162
Θ_z	90.0	-118.7	90.0	107.2	67.9	106.2	73.4
ΔE	-	0.0	3.8	1.0	0.0	0.7	0.0

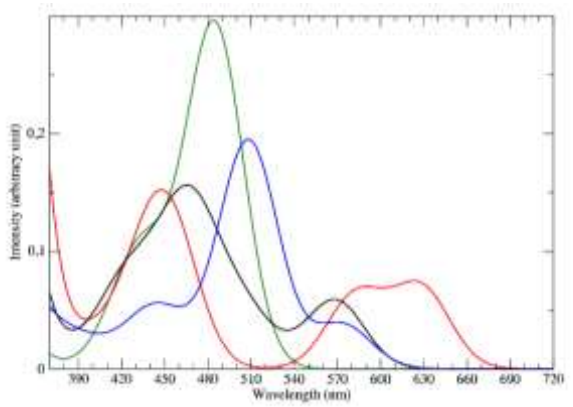

Figure 7. Theoretical absorption spectra in the visible domain for complexes **C1** (black trace), **C2** (blue trace), $[Cu(dipp)_2]^+$ (green trace) and $[Cu(dpp)_2]^+$ (red trace) on the RX structures

The theoretical spectrum of **C1** mostly reproduces the characteristics of the experimental one; the main band is located at 466 nm with again smaller intensity transitions between 500-600 nm and corresponding to the lowest singlet excited states calculated at 569, 532, 504 and 500 nm. The absorption spectrum of **C2** is characterized by three peaks at 445, 510 and 570 nm. The most intense band at 510 nm is generated by two singlet states calculated at 506 and 512 nm. The presence of accessible conformers may explain the discrepancies between theoretical and experimental absorption spectra.

The spectra computed on the *conf* structures present significant shift of the bands. For the $[Cu(dpp)_2]^+$ complex, the *conf* structure leads to tetrahedral arrangement around the copper cation and the spectrum is very similar to that of $[Cu(dipp)_2]^+$ complex, illustrating again the structural impact on the optical properties (figure S14). Moreover, these results prove as well that the *conf* structure of $[Cu(dpp)_2]^+$ does not participate in its absorption spectrum. For **C1** and **C2** complexes, the differences between the *RX* (Figure 7) and *conf* spectra (Figures S15 and S16) are less drastic though significant, revealing that both structures are substantially participating in the overall optical properties. As for our previous work on the $[Cu(phenX_2)_2]^+$ complexes (where $phenX_2$ stands for 2,9-diX-1,10-phenanthroline and X = Cl, Br or I),[22] the present complexes are highly flexible and present several minima that can contribute to the absorption spectrum. The limitation of the static approach, which does not reflect this flexibility, explains the difference between the experimental and theoretical results. The influence of the dynamics on the absorption spectrum of **C2**, which are known to strongly influence the latter, are likely responsible for the differences between the experimental and calculated spectra. Importantly, the calculations match with the experimentally observed trend that the extinction coefficients of the $S_0 \rightarrow S_n$ transitions decrease when phenyl groups are tethered in α of the nitrogen atoms of phenanthroline.[23]

Emission spectra

Nuclear evolution, mainly the Θ_z angle (as defined in figure S4) and the Cu-N distances, and electronic re-localization underlie excited state relaxation. Delocalization of the excited electron over the two phenanthroline ligands corresponds to D_2 point group for $[Cu(dipp)_2]^+$ and $[Cu(dpp)_2]^+$ complexes and to C_2 point group for **C1** and **C2** complexes. Localization on one phenanthroline only leads to C_2 point group for $[Cu(dipp)_2]^+$ and $[Cu(dpp)_2]^+$ complexes and to C_1 point group for **C1** and **C2** complexes (see figure S17 and table ST3).

$[Cu(dipp)_2]^+$

For $[Cu(dipp)_2]^+$, two symmetry point groups were considered, D_2 allowing the flattening of the complex and C_2 allowing the electronic localization on one of the ligand (figure S17 and table ST3). We retrieve similar results as for the $[Cu(phenX_2)_2]^+$ complexes series.[22] The lowest energy structures belong to the C_2 symmetry with singlet and triplet states of MLCT character (Figure 8, right). However, the lowest singlet and triplet states of D_2 symmetry are very close in energy (Table 4) and correspond to transition states on the C_2 potential energy profile joining the two minima. Whereas the triplet emission wavelength (C_2 and D_2) are underestimated as compared to the experimental values, the emission wavelength of the lowest singlet state of D_2 symmetry (first singlet of B1 symmetry) agrees with the experiment (calculated 673 nm in table 4 vs. measured 679 nm in table 2). Similarly to the $[Cu(phenX_2)_2]^+$ complexes and as observed experimentally in usual homoleptic[5b, 22, 24] and heteroleptic copper(I) complexes[25] a thermally activated delayed fluorescence (TADF) is proposed. Indeed, SOC and ΔE_{ST} are favorable to an efficient re-population of the singlet potential energy surface (PES) after relaxation in the lowest triplet PES. Molecular oscillatory motion between the two minima of C_2 symmetry characterizes the dynamics of the system in both PES. This results in a structure that is, in average, of D_2 symmetry, which can be considered as the emitting one. This is further supported by the respective oscillator strength of the singlet states in the C_2 (S1A) and D_2 (S1B1) symmetry. There is one order of magnitude in favor of the D_2 structure (Figure 8).

Table 4. Computed emission wavelength (in nm), Singlet-Triplet energy splitting (ΔE_{ST} in eV) at the geometry of the triplet state and Spin-Orbit Coupling (SOC in cm^{-1}) at the same geometry for $[Cu(dipp)_2]^+$ complex in the D_2 and C_2 point groups, energetic barrier (in cm^{-1}) between the D_2 geometry and the C_2 minima, flattening of structure (Θ_z in degrees) and oscillator strength of the singlet state.

Symmetry	D_2		C_2	
State	S1B1	T1A	S1A	T1A
λ_{em}	673	861	760	914
ΔE_{ST}		0.332		0.336
SOC		18.2		56.8
barrier	736	502	0	0
Cu-N_A	2.039	2.017	1.992	1.992
Cu-N_B	2.039	2.017	2.116	2.063
Θ_z	-110.0	-108.9	110.1	110.9
f_{osc}	7.9 10^{-2}		1.7 10^{-2}	

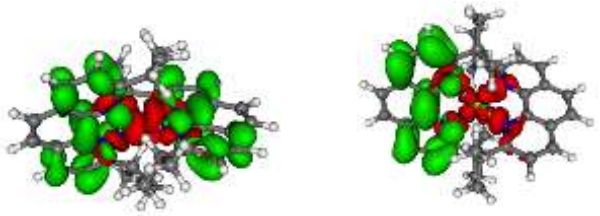

D_2 **C_2**

Figure 8. Electronic density difference between ground and excited states of T1a states of D_2 symmetry (left) and of C_2 symmetry (right) of the $[Cu(dipp)_2]^+$ complex. In red and green are the electron depleted and enriched zones respectively.

$[Cu(dpp)_2]^+$

The structures of the excited states generated by the *conf* structure of $[Cu(dpp)_2]^+$ complex are much less stable than those from the *RX* conformer and will not be detailed further (See table ST4). The *RX* structures are already flattened in the ground state (Θ_z=-119.7°) and almost no extra flattening is observed in the excited state geometries which justifies its particularly good photophysical behavior.[26] Similarly to $[Cu(dipp)_2]^+$ complex, the triplet emission wavelengths are incompatible with the experimental data (Table 5, Table 2) while the singlet emission wavelength (D_2 symmetry) reproduces rather well the experiment leading to a nearly identical photophysical mechanism.

For $[Cu(dipp)_2]^+$ and $[Cu(dpp)_2]^+$ complexes only two geometrical distortions are observed upon excitation. We observe a variation of the Θ_z angle due to the flattening of the ligand and variation of the Cu-N distances. Those distances are reduced for the ligand accepting the excited electron and lengthened for the inert ligand. No rocking nor wagging is observed.

C1 and C2

Complexes **C1** and **C2** in their excited states are characterized by several conformers close in energy with similar emission wavelengths (table 6 and table 7). The singlet and triplet emission wavelengths generated by the structures of C_1 symmetry disagree with the experimental data. The same conclusion can be drawn for the emission from the structures of C_2 symmetry in their triplet state. However, the emission wavelength computed for the S1B singlet states of C_2 symmetry is in very good agreement with the experiment regardless of the considered conformer *RX* or *conf*.

As for $[Cu(dpp)_2]^+$, **C1** and **C2** present a flattening in the ground state (Table 3) due to intramolecular π-stacking interactions. The extra flattening generated by the excitation is small but larger for the *RX* structures (around 7°) than for the *conf* structures (around 3°).

Table 5. Emission wavelength (in nm), Singlet-Triplet energy splitting (ΔE_{ST} in eV) at the geometry of the triplet state and Spin-Orbit Coupling (SOC in cm^{-1}) at the same geometry for $[Cu(dpp)_2]^+$ complex in the D_2 and C_2 point groups, energetic barrier (in cm^{-1}) between the D_2 geometry and the C_2 minima, flattening of structure (Θ_z in degrees) and oscillator strength of the singlet state.

Symmetry	D_2		C_2	
State	S1B1	T1A	S1A	T1A
λ_{em}	698	905	754	949
ΔE_{ST}		0.331		0.353
SOC		15.3		49.5
Barrier	252	445	0	0
Cu-N_A	2.041	2.007	1.995	1.988
Cu-N_B	2.041	2.007	2.106	2.055
Θ_z	-120.7	-121.3	-121.0	-120.9
f_{osc}	6.3 10^{-2}		2.8 10^{-2}	

Table 6. Emission wavelength (in nm), Singlet-Triplet energy splitting (ΔE_{ST} in eV) at the geometry of the triplet state and Spin-Orbit Coupling (SOC in cm^{-1}) at the same geometry for **C1** complex in the C_2 and C_1 point groups, energetic barrier (in cm^{-1}) between all geometries and the RX C_1 minima, flattening of structure (Θ_z in degrees) and oscillator strength of the singlet state.

Symmetry	C_2(RX)		C_1(RX)		C_2(conf)		C_1(conf)	
State	S1B	T1A	S1	T1	S1B	T1A	S1	T1
λ_{em}	684	894	757	939	679	892	764	933
ΔE_{ST}		0.354		0.355		0.334		0.363
SOC		17.7		48.8		13.6		52.5
barrier	401	354	0	35	485	596	8	0
Cu-N_{1A}	2.057	2.022	2.009	1.997	2.046	2.005	1.974	1.977
Cu-N_{2A}	2.036	2.010	1.983	1.986	2.040	2.023	2.006	2.007
Cu-N_{1B}	2.057	2.022	2.160	2.083	2.046	2.005	2.160	2.061
Cu-N_{2B}	2.036	2.010	2.072	2.043	2.040	2.023	2.072	2.059
Θ_z	114.8	114.2	113.8	114.4	65.0	65.1	67.2	64.4
f_{osc}	6.9 10^{-2}		2.2 10^{-2}		6.9 10^{-2}		1.8 10^{-2}	

The asymmetry in the substituents of the phenanthroline ligand is reflected in the different Cu-N distances. For **C1**, the Cu-N_1 distances are longer than the Cu-N_2 distances. This is reversed for **C2**. This is easily explained; in **C2** the longer Cu-N_2 distance is due to the steric repulsion generated by the *tert*-butyl moiety which is larger than isopropyl. The evolution of these distances in **C1** and **C2** in the excited state depends if the molecule is excited from the *RX* or from the *conf* structure. The most noticeable point is the evolution of the Cu-N_{2B} distances in the *conf* conformer of

C2. It rises up to 2.4 Å in the *C1* point group symmetry (Table 7) potentially opening the way for partial ligand decoordination.

Table 7. Emission wavelength (in nm), Singlet-Triplet energy splitting (ΔE_{ST} in eV) at the geometry of the triplet state and Spin-Orbit Coupling (SOC in cm^{-1}) at the same geometry for **C2** complex in the *C2* and *C1* point groups, energetic barrier (in cm^{-1}) between all geometries and the RX C_1 minima, flattening of structure (Θ_z in degrees) and oscillator strength of the singlet state.

Symmetry	*C2*(RX)		*C1*(RX)		*C2*(conf)		*C1*(conf)	
State	S1B	T1A	S1	T1	S1B	T1A	S1	T1
λ_{em}	662	830	815	925	650	781	793	910
ΔE_{ST}		0.339		0.270		0.287		0.250
SOC		35.5		63.4		32.9		56.9
barrier	1460	891	421	239	933	823	0	0
Cu-N_{1A}	2.096	2.057	1.995	2.002	2.006	1.982	1.980	1.971
Cu-N_{2A}	2.045	2.027	1.994	2.003	2.149	2.138	1.993	1.995
Cu-N_{1B}	2.096	2.057	2.212	2.176	2.006	1.982	2.057	2.026
Cu-N_{2B}	2.045	2.027	2.130	2.060	2.149	2.138	2.421	2.390
Θ_z	111.0	111.5	98.8	113.4	68.3	71.6	74.8	72.0
f_{osc}	5.2 10^{-2}		1.5 10^{-3}		5.6 10^{-2}		6.9 10^{-3}	

The presence of a flexible non symmetrical ligand generates several minima on the lowest excited singlet and ground and lowest excited singlet and triplet states PES. This conformational flexibility has to be taken into account to reproduce the experimental result, as the different conformers will be present in the solution due to their close stability. This affects the calculation of the absorption and emission spectra and may be the source of the large band observed for the emission. The excitation can localize on one of the two ligands. However, the energy of the symmetric structure, which is the transition state between the two minima, is so low that in reality the complexes freely oscillate in between those two minima. As a consequence, in average the structure is symmetric and explains the very good agreement between the computed and experimental emission wavelengths for the symmetric structures for all complexes. The value computed for the triplet-singlet splitting (ΔE_{ST}), between 0.3-0.4 eV and the spin-orbit coupling (SOC) values are compatible with the TADF mechanism but from a structure that is not an energy minimum. From this point of view the rather large ΔE_{ST} is compensated not only by SOC but also by vibronic coupling effects.[27] The presence of phenyl rings on the phenanthroline ligand induces a flattening of the structure in the ground state, which is almost identical in the excited states: no further flattening is observed. This invalidates the hypothesis that the non-symmetrical nature of the ligands is responsible for extra flattening of the coordination sphere upon excitation.

The computed energies of the excited state (see table ST5) correlate well with those measured by the tangent method whether the *conf* or *RX* structures are considered for **C1** and **C2**. This confirms that increasing the steric burden around the copper ion allows indeed to rise the energy gap between S_1 and the ground state.

The theoretical results have shown that the decrease in absorption for $[Cu(dpp)_2]^+$, **C1** and **C2** is due to the initial flattening of the complexes induced by the phenyl moieties. We also put in evidence that dynamically the excited state is delocalized over two ligands. However, none of the discussed above characteristics are responsible for the emission intensity drop of **C1**, **C2** and $[Cu(dpp)_2]^+$ compared to $[Cu(dipp)_2]^+$. One last movement has to be considered. Upon excitation, the initially D_{2d} $[Cu(dipp)_2]^+$ complex flattens generating two degenerated conformers (see figure S18). We found a transition state connecting these two conformers on the lowest triplet PES with a relatively low associated energy barrier (computed ΔG = 3.5 kcal.mol^{-1}). At this geometry, in which Θ_z is almost 90°, the coupling between S_0 and S_1 is very small (it is strictly nil in the ground state *D2d* structure). The emission of $[Cu(dipp)_2]^+$ is relatively intense because it arises from a flattened conformation. The observed stabilizing interactions between the ligand for $[Cu(dpp)_2]^+$, **C1** and **C2** (which hold while shifting from one energy well to the other) may lower this barrier so that dynamically, an orthogonal structure significantly contributes to the emission properties. As a consequence, the reverse intersystem crossing channel would be less favorable, decreasing the TADF efficiency and leading to the less intense emission for these complexes compared to that of $[Cu(dipp)_2]^+$ complex (for which such structure is too high in energy).

Overall, complexes **C1** and **C2** stand out in the series of complexes by the fact that many different but equally probable structures are in dynamic equilibrium, and this opens many non-radiative pathways which entail a significant increase of k_{nr} and thus weaker emission quantum yields.

Stability studies

Given the lability of the copper(I)-phenanthroline coordination sphere, the stability of the complexes is strongly impacted by the steric bulk around the metal ion. For example, $[Cu(dtbp)_2]^+$ is quantitatively destroyed in presence of one equivalent of acetonitrile[5a] thanks to a strong steric relief. We thus began by recording the ^{1}H NMR spectrum of **C1** and **C2** in deuterated acetonitrile. **C1**'s spectrum featured the expected signals of the homoleptic complex, and the spectra remained unchanged for several weeks (figure S19). On the other hand, the ^{1}H NMR spectrum of **C2** revealed the latter is in equilibrium with other species (figure S20). Indeed, the UV-Vis spectrum of **C2** in dichloromethane is strongly affected by the addition of aliquots of CH_3CN (figure S21), the MLCT significantly collapsing upon increasing the acetonitrile's concentration while some weak absorbance over the visible range confirms the formation of a $[Cu(\mathbf{L_2})(CH_3CN)]^+$ species following equation 2:

$[Cu(\mathbf{L2})_2]^+ + 2CH_3CN \rightarrow [Cu(\mathbf{L2})(CH_3CN)_2]^+ + \mathbf{L2}$ (equation 2)[19, 28]

This is not unexpected since the *tert*-butyl group leads to longer Cu-N_{2A} and Cu-N_{2B} distances and limits the extent of stabilizing intramolecular π-stacking.

Interestingly, **C1**'s spectrum was slightly affected by acetonitrile too revealing some instability for dilute solutions, while $[Cu(dipp)_2]^+$ and $[Cu(dpp)_2]^+$ spectra remained roughly idle in the same conditions (figures S22 and S23). This prompted us to inquire further about the behaviour of our complexes in presence of nucleophiles.

Stopped flow analysis

Monitoring the real time decomplexation of copper(I) complexes by cyanide by stopped flow is a valuable tool to study the accessibility of copper(I) towards nucleophilic attacks, and how shielded is the latter by the groups tethered in α of the nitrogen atoms of phenanthroline. The process is based on the chemical equation:

$$Cu(NN)_2^+ + 4\ CN^- \rightarrow Cu(CN)_4^{3-} + 2NN \quad \text{(equation 3)}$$

The huge complexation constant of $Cu(CN)_4^{3-}$ (10^{28} vs. 10^{10-12} for $Cu(NN)_2^+$ complexes) is the main driving force for this quantitative demetallation reaction.[29] Complexes bearing non-symmetrical phenanthroline ligands have previously shown enhanced kinetics towards cyanide assisted demetallation compared to symmetrical systems.[19] Willing to assess if the behaviour of **C1** and **C2** in those conditions would follow the same trend, the decay of the MLCT with time in presence of excess CN^- in a 1:1 (v/v) dichloromethane:acetonitrile mixture was monitored by stopped flow. $[Cu(dipp)_2]^+$ and $[Cu(dpp)_2]^+$ were studied in the same conditions for comparison purpose.

C2 proved to be too unstable in the solvent mixture and was therefore not further examined. In all other cases, decays are monoexponential with measured decay constants k_{obs} (figure S24). In our experimental conditions (large excess of tetrabutylammonium cyanide) the degradation kinetics can be considered as pseudo first order in complex. Plots of k_{obs} vs. $[CN^-]$ yield straight lines (figure S25). The intersection with vertical axis affords the constant k_D insensitive to $[CN^-]$ and assigned to the natural dissociation kinetics of the complexes in the analysis medium.[18-19] The slopes of the straight lines yields the constant k_{CN} assigned to cyanide assisted demetallation. Significant values of k_{CN} indicate that cyanide is involved in the rate determining step (figure S26). Constants are given in table 8 and experimental details can be found in the SI (table ST6).

Table 8. Dissociation rate constants of copper(I) bis(diimine) complexes **C1**, $[Cu(dpp)_2]^+$ and $[Cu(dipp)_2]^+$ in acetonitrile, with $[Bu_4NPF_6]$ = 0.05 M; T = 25.0 ± 0.2 °C.

Complexes	k_D (s^{-1})	k_{CN}($M^{-1}s^{-1}$)
$Cu(dpp)_2^+$	0.976 ± 0.07	11.50 ± 0.08
$Cu(dipp)_2^+$	0.30 ± 0.04	229 ± 4
C1	14 ± 5	8526 ± 551

In line with previously published results,[19, 29] $[Cu(dpp)_2]^+$ is the more resilient species vs. cyanide demetallation thanks to the intramolecular π-stacking interactions between the phenyl and the vicinal phenanthroline: the copper(I) ion is well protected in this rigid cavity, as incidentally evidenced by its good photophysical properties in strongly coordinating medium. $[Cu(dipp)_2]^+$ is deprived of stabilizing interactions and therefore more prone to react with cyanide, as indicated by a ca. 20 times larger k_{CN} compared to $[Cu(dpp)_2]^+$. As previously observed for complexes bearing non-symmetrically substituted phenanthroline ligands, **C1** features a larger k_{CN} than $[Cu(dpp)_2]^+$ by almost two orders of magnitude, revealing that the non-symmetrical nature of **L1** promotes cyanide nucleophilic attack on the copper ion.[19] Less intuitively, k_{CN} is also much larger for **C1** than for $[Cu(dipp)_2]^+$ despite an intermediate steric hindrance. However, this is in line with the behavior hypothesized in the literature: the non-symmetrical nature of the ligands provides a protected side by stacking of the phenyl group which simultaneously opens a site on the other side of the complexes, explaining their enhanced reactivity towards cyanide (and acetonitrile).

k_D values reflect the fact that acetonitrile can behave as a competitor ligand, leading to partial dissociation of the complexes. k_D increases in the order $[Cu(dipp)_2]^+ < [Cu(dpp)_2]^+ <<$ **C1**: this means that **C1** dissociates faster than $[Cu(dpp)_2]^+$ and $[Cu(dipp)_2]^+$ in acetonitrile, which is in line with the conclusions from the cyanide induced decomplexation. The fact that $[Cu(dpp)_2]^+$ dissociates faster than $[Cu(dipp)_2]^+$ is unexpected; we propose that the electron-withdrawing character of phenyl depletes the σ-donating power of dpp compared to dipp (where electron rich isopropyl groups have the opposite effect) and this could translate into the (slightly) faster dissociation of $[Cu(dpp)_2]^+$. As a conclusion, the observation that complexes bearing non symmetrical phenanthroline are more prone to nucleophilic attack than classical complexes with symmetrically substituted ligands can be relevantly compared to their enhanced exciplex quenching. This fragility in the ground state is likely exacerbated in the excited state.

Reactivity

Using the Rehm and Weller equation, it is possible to estimate the reductive and oxidative power of photosensitizers promoted in their excited state, namely E(**Cn**$^+$/**Cn***) and E(**Cn***/**Cn**$^-$) (or E_{ox}*) for **C1** and **C2**. Considering the case of E_{ox}*, the Rehm and Weller equation gives:

$$E_{ox}^* = E(\mathbf{Cn}/\mathbf{Cn}^-) + E^{00} \quad \text{(equation 4)}$$

Where E(**Cn**/**Cn**$^-$) is the reduction potential of complexes **Cn** (E_2 in table 1) and E^{00} is the energy of the excited state. Both **C1** and **C2** exhibit more positive E_{ox}* than $[Cu(dpp)_2]^+$, and comparable to $[Cu(dipp)_2]^+$. Thus, the driving force for photo-induced electron transfers is more favorable for **C1** and **C2** than for the model complex $[Cu(dpp)_2]^+$. In order to test this assertion, we decided to try and implement reductive quenching with **C1** and **C2** with decamethylferrocene (dmFc) as electron donor (figure 9). The latter is an excellent donor (E($dmFc^+$/dmFc) = -0.57 V vs. Fc^+/Fc) which has been successfully used by McMillin et al. in what are, to the best of our knowledge, the only articles ever reporting reductive quenching with homoleptic $[Cu(NN)_2]^+$ complexes (namely $[Cu(dipp)_2]^+$ and $[Cu(dpp)_2]^+$).[10, 30] Indeed, the latter are particularly poor photo-oxidants.[1a] Yet, successfully performing reductive quenching with plain homoleptic copper(I) complexes is a valuable endeavor leading to the photo-generation of very reductive species $[Cu(NN)_2]^0$ (more precisely $[Cu^I(NN)(NN^{\bullet-})]^0$) paving the way towards low-cost, visible light-activated photo-reduction processes of difficult substrates or catalysts. We however highlight that the reversibility of the $dmFc^+$/dmFc couple prevents accumulation of **Cn**$^-$ upon photoexcitation (figure 9, step 3).

10.1002/chem.202001209

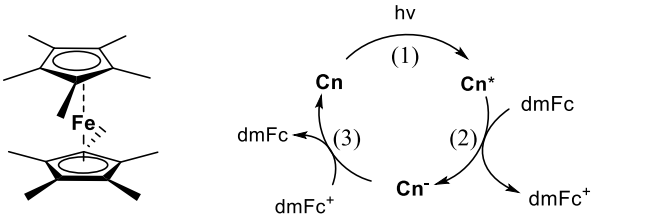

Figure 9. The reductive quenching cycle in the case of **Cn** (n = 1 or 2) as photosensitizer and dmFc as electron donor.

Using the same experimental protocol than McMillin et al.,[30] we monitored the impact of increasing quantities of dmFc in dichloromethane solutions of **C1**, **C2**, $[Cu(dpp)_2]^+$ and $[Cu(dipp)_2]^+$ on their luminescence lifetime and extracted bimolecular quenching rates k_Q using Stern-Volmer formalism (figure S27). Importantly, the quenching of the excited state of all copper complexes may occur *via* two mechanisms: energy transfer ("EnT" from MLCT excited state to low lying iron(II) based dd states, kinetic constant k_{EnT}) and electron transfer (from dmFc to excited copper complexes, namely reductive quenching, kinetic constant k_{RQ}). Thus, $k_Q = k_{RQ} + k_{EnT}$. As previously demonstrated, k_{EnT} can be considered similar for plain ferrocene and dmFc since the energies of the final quencher d-d state are similar.[30-31] Electron transfer processes between ferrocene and copper complexes being thermodynamically uphill, one can roughly estimate k_{EnT} ($k_Q = k_{EnT}$ when the quencher is plain ferrocene Fc) by monitoring copper complexes luminescence quenching by plain ferrocene (figure S28, table ST7). As previously observed, quenching by energy transfer is one order of magnitude less efficient than quenching by photo-induced electron transfer, making the latter the dominant phenomenon in presence of dmFc. Thus, we could estimate k_{RQ} and the results are reported in table 2: **C1** and **C2**'s emissions are more efficiently quenched by dmFc than $[Cu(dpp)_2]^+$, meaning that **C1** and **C2** are more efficient photo-oxidants than $Cu(dpp)_2^+$, k_{RQ} being twice and three times larger for **C1** and **C2** respectively than $k_{RQ}([Cu(dpp)_2]^+)$. Interestingly k_{RQ}(**C1**) is smaller than $k_{RQ}([Cu(dipp)_2]^+)$ or k_{RQ}(**C2**) although those three complexes have comparable photo-oxidative powers from the sole thermodynamic point of view (see E_{ox}* table 2). This is certainly due to kinetic factors. Indeed, the latter are believed to be particularly prominent for reductive quenching,[8c, 30] because the complex shifts from a flattened excited state toward a tetrahedral reduced copper(I) complex (figure 9, step 2) whereas it shifts from a flattened excited state to a flattened oxidized copper(II) complex in the frame of oxidative quenching. The reorganization energy is thus supposed to be a particularly important factor to take into account here; given our results, **C1** and **C2** should thus display higher reorganization energies. However, computed distortion energies do not reflect the observed trend (table ST5) as $[Cu(dipp)_2]^+$ exhibits larger reorganization energies than **C1** and **C2** for the computed states (due to the flattening movement contribution which is more prominent that in the three other complexes). Work is ongoing to rationalize this observation.

Conclusions

The use of non-symmetrical phenanthroline ligands bearing one phenyl and one ramified alkyl chain to respectively stabilize and sterically strain corresponding copper(I) complexes is reported. Tethering an isopropyl or a tert-butyl chain and a phenyl group in α of the nitrogen atoms allowed to implement intramolecular π stacking interactions and rise the complex excited state energy at the same time by ca. 100 meV compared to symmetrical $[Cu(dpp)_2]^+$. Calculations reveal that the stacking interactions lead to a more rigid coordination sphere for **C1** and **C2**, the extent of computed photo-induced flattening being smaller than for $[Cu(dipp)_2]^+$ where no stacking takes place. The stacking was nevertheless not sufficient to stabilize the coordination sphere when using *tert*-butyl instead of isopropyl substituents, because of the strong steric strain imposed by the tertiary ramified alkyl chain.

The unsymmetrical nature of the phenanthroline ligand promotes nucleophilic attacks on the copper centre in **C1** and **C2** in their ground states. We extend this statement to the excited state, exciplex quenching being more efficient for non-symmetrical complexes, and thus rationalize their rather weak photophysical parameters (emission quantum yield and lifetime). Simulation of the emission wavelengths was achieved with TD-DFT calculations. Importantly, the fitting required to take into account that the electron in the MLCT excited state oscillates between the two ligands, leading to an overall symmetrical potential well. The increased energy of the excited state for **C1** and **C2** lead to better photo-oxidizing power, which materialized in improved reductive quenching kinetics compared to $[Cu(dpp)_2]^+$.

Experimental Section

General: chemicals were purchased from Sigma-Aldrich or Fisher Scientific and used as received. Thin-layer chromatography (TLC) was performed on aluminium sheets precoated with Merck 5735 Kieselgel 60F254. Column chromatography was carried out with Merck 5735 Kieselgel 60F (0.040-0.063 mm mesh). ^{1}H spectra were recorded on an AVANCE 300 UltraShield BRUKER. Chemical shifts for ^{1}H NMR spectra are referenced relative to residual protium in the deuterated solvent ($CDCl_3$ δ = 7.26 ppm). NMR spectra were recorded at room temperature, chemical shifts are written in ppm and coupling constants in Hz. Mass spectrometry was performed with a JEOL JMS-700 B/E spectrometer. Electrochemical measurements were made under an argon atmosphere in CH_2Cl_2 with 0.1 M Bu_4NPF_6. Cyclic voltammetry experiments were performed by using an Autolab PGSTAT 302N potentiostat/galvanostat. A standard three-electrode electrochemical cell was used. Potentials were referenced vs. reversible ferrocenium/ferrocene couple. The working electrode was a glassy carbon disk and the auxiliary electrode was a Pt wire. UV-visible absorption spectra were recorded on an Analytik Jena spectrophotometer, using 1 cm path length cells. Emission spectra were recorded on a Fluoromax-3 Horiba spectrofluorimeter (1 cm quartz cells). E00 values were measured by the tangent method: a tangent to the emission spectrum was drawn on the blue side of the latter and the intersection with the baseline gives wavelength λ^{00}, used to calculate $E^{00} = 1240/\lambda^{00}$. Luminescence decays were recorded with a DELTAFLEX time correlated single photon counting system (HORIBA) on degassed dichloromethane solutions. X-ray single-crystal diffraction data for **L1** were collected at 150K on a Rigaku Oxford Diffraction SuperNova diffractometer equipped with Atlas CCD detector and micro-focus Cu-Kα radiation (λ = 1.54184 Å). The structure was solved by direct methods and refined on F2 by full matrix least-squares techniques using SHELX programs (G. M. Sheldrick 2013-

2016, SHELXS 2013/1 and SHELXL 2016/4). All non-H atoms were refined anisotropically and multiscan empirical absorption was corrected using CrysAlisPro program (CrysAlisPro, Agilent Technologies, V1.171.38.46, 2015). The H atoms were included in the calculation without refinement. CCDC-1972177 contains the supplementary crystallographic data for this paper. Crystallographic data: $C_{22}H_{20}N_2$, M = 312.40, colorless prism, 0.326 x 0.298 x 0.254 mm3, orthorhombic, space group P212121, a = 9.7972(1) Å, b = 11.6086(2) Å, c = 15.1268(2) Å, V = 1720.40(4) Å3, Z = 4, ρcalc = 1.206 g/cm3, μ = 0.543 mm-1, F(000) = 664, θmin = 4.802 °, θmax = 76.289°, 6751 reflections collected, 3339 unique (Rint = 0.0252), parameters / restraints = 221 / 0, R1 = 0.0419 and wR2 = 0.1117 using 3278 reflections with I>2σ(I), R1 = 0.0445 and wR2 = 0.1155 using all data, absolute structure parameter = 0.2(3), GOF = 1.041, -0.250 < Δρ < 0.387 e.Å-3. X-ray single-crystal diffraction data for C2 were collected at 150K on a D8 VENTURE Bruker AXS diffractometer equipped with a (CMOS) PHOTON 100 detector, Mo-Kα radiation (λ = 0.71073 Å, multilayer monochromator). Crystallographic data: ($C_{44}H_{40}CuN_4$•F_6P•2(C_7H_8)); M = 1017.57. monoclinic P 21/n (I.T.#14), a = 14.9886(15), b = 19.446(2), c = 17.4437(15) Å, β = 105.329(3) °, V = 4903.3(8) Å3. Z = 4, d = 1.378 g.cm-3, μ = 0.545 mm-1. The structure was solved by dual-space algorithm using the SHELXT program,[32] and then refined with full-matrix least-squares methods based on F2 (SHELXL).[33] All non-hydrogen atoms were refined with anisotropic atomic displacement parameters. H atoms were finally included in their calculated positions and treated as riding on their parent atom with constrained thermal parameters. A final refinement on F2 with 11112 unique intensities and 639 parameters converged at ωRF2 = 0.1231 (RF = 0.0500) for 8360 observed reflections with I > 2σ(I).
Stopped Flow absorption spectrophotometry was performed on a BioLogic SFM-4000 coupled to a J&M Tidas diode array spectrometer. Experiments were at least triplicated for kinetic fits. Monoexponential fits were performed using the Biokine software (BioLogic).

2-(*tert*-butyl)-1,10-phenanthroline (1) Under argon, the 1,10-phenanthroline (1.00 g, 5.56 mmol) is dissolved into dry toluene (48 mL). The solution is cooled to 0°C before addition dropwise of *tert*-butyllithium (1.7 M, 4.9 mL). The resulting solution was allowed to warm to room temperature and stir for 18 h. Water (10 mL) was then added followed by a dichloromethane extraction. Organics phases are stirred with activated manganese dioxide (12.00 g, 139.00 mmol) for 6h. The mixture was dried over magnesium sulfate, filtrated and evaporated. The orange oil is chromatographed on silica column (0 to 5% of methanol in dichloromethane) to obtain 931 mg (71%) of the product. ^{1}H NMR spectrum (300MHz, $CDCl_3$) δ= 9.23 (dd, $^4J_{H,H}$=1.8Hz, $^3J_{H,H}$=4.5Hz, 1H), 8.24 (dd, $^4J_{H,H}$=1.8Hz, $^3J_{H,H}$ = 8.1Hz, 1H), 8.19 (d, $^3J_{H,H}$ = 8.4Hz, 1H), 7.78 (m, 3H), 7.62 (dd, $^3J_{H,H}$= 4.5Hz, $^3J_{H,H}$= 8.1Hz, 1H), 1.61 (s, 9H). ^{13}C NMR spectrum (75MHz, $CDCl_3$) δ= 169.80 (s), 150.38 (s), 146.53 (s), 145.00 (s), 136.10 (s), 128.93 (s), 126.72 (s), 126.41 (s), 125.62 (s), 122.43 (s), 119.95 (s), 38.66 (s), 30.51 (s). HRMS (ESI$^+$) for $C_{16}H_{16}N_2$ $[M+H]^+$, *m/z* 237.1399 found, 237.1392 calc.

2-isopropyl-1,10-phenanthroline (2) was synthesized in a similar manner to that of (1) using the following reagents: 1,10-phenanthroline (200 mg, 1.11 mmol), isopropyllithium (0.7 M, 2.4 mL) and manganese dioxyde (2.40 g, 27.8 mmol). Yield: 174 mg (71%). ^{1}H NMR spectrum (400MHz, $CDCl_3$) δ= 9.25 (dd, $^4J_{H,H}$ = 1.6Hz, $^3J_{H,H}$ = 4.4Hz, 1H), 8.25 (m, 2H), 7.78 (AB, J_{AB}= 15.6Hz, 2H), 7.64 (m, 2H), 3.69 (sept, $^3J_{H,H}$ = 7.2Hz, 1H), 1.49 (d, $^3J_{H,H}$ = 7.2Hz, 6H). ^{13}C NMR spectrum (100MHz, $CDCl_3$) δ= 206.82 (s), 150.34 (s), 145.41 (s), 136.58 (s), 135.99 (s), 126.47 (s), 125.56 (s), 122.61 (s), 120.05 (s), 37.71 (s), 30.89 (s), 23.16 (s). HRMS (ESI$^+$) for $C_{15}H_{14}N_2$ $[M+H]^+$, *m/z* 223.1243 found, 223.1235 calc.

2-isopropyl-9-phenyl-1,10-phenanthroline (**L1**) was synthesized in a similar manner to that of (1) using the following reagents: (2) (174 mg, 0.78 mmol), phenyllithium (1.9 M, 0.62 mL) and manganese dioxide (1.69 g, 19.50 mmol). Yield: 224 mg (96%). All characterization data are in agreement with the ones published by Kavita et al.[11]

2-(*tert*-butyl)-9-phenyl-1,10-phenanthroline (**L2**) was synthesized in a similar manner to that of (1) using the following reagents: (1) (100 mg, 0.42 mmol), phenyllithium (2.0 M, 0.32 mL) and manganese dioxide (912 mg, 10.5 mmol). Yield: 117 mg (89%). ^{1}H NMR spectrum (300MHz, $CDCl_3$) δ= 8.48 (m, 2H), 8.30 (d, $^3J_{H,H}$ = 8.7Hz, 1H), 8.18 (d, $^3J_{H,H}$ = 8.7Hz, 1H), 8.15 (d, $^3J_{H,H}$ = 8.4Hz, 1H), 7.77 (m, 3H), 7.57 (m, 2H), 7.47 (m, 1H), 1.64 (s, 9H). ^{13}C NMR spectrum (75MHz, $CDCl_3$) δ= 156.34 (s), 139.43 (s), 136.84 (s), 136.05 (s), 129.39 (s), 128.82 (s), 127.42 (s), 126.99 (s), 126.08 (s), 125.34 (s), 120.08 (s), 119.24 (s), 38.76 (s), 30.36 (s). HRMS (ESI$^+$) for $C_{22}H_{20}N_2$ $[M+H]^+$, *m/z* 313.1714 found, 313.1705 calc.
Anal. Calcd for $C_{22}H_{20}N_2$. 0.05 CH_2Cl_2 . 0.05 C_5H_{12} : C, 83.63; H, 6.51; N, 8.75. Found: C, 83.31; H, 6.19; N, 8.53.

[Cu(L1)$_2$]PF$_6$ (**C1**) Under argon atmosphere, $[Cu(ACN)_4]PF_6$ (58 mg, 0.16mmol) was dissolved in 4mL of degassed dichloromethane. This solution was transferred into a vial that contains **L1** (92 mg, 0.31mmol). The red resulting solution was stirred overnight at room temperature. The mixture was precipitate in hexanes to obtain a red powder (100%, 248mg) ^{1}H NMR spectrum (300MHz, $CDCl_3$) δ= 8.59 (d, $^3J_{H,H}$= 8.4Hz, 2H), 8.52 (d, $^3J_{H,H}$= 8.4Hz, 2H), 8.04 (s, 4H), 7.94 (d, $^3J_{H,H}$= 8.4Hz, 2H), 7.72 (d, $^3J_{H,H}$= 8.4Hz, 2H), 7.24 (m, 4H), 6.69 (t, $^3J_{H,H}$= 7.5Hz, 2H), 6.37 (d, $^3J_{H,H}$= 7.8Hz, 4H), 3.21 (t, $^3J_{H,H}$ = 6.9Hz, 2H), 1.13 (d, $^3J_{H,H}$= 7.2Hz, 6H), 0.92 (d, $^3J_{H,H}$= 6.9Hz, 6H). ^{13}C NMR spectrum (125MHz, $CDCl_3$) δ= 166.42 (s), 157.67 (s), 143.77 (s), 142.85 (s), 139.03 (s), 137.85 (s), 137.81 (s), 128.63 (s), 128.38 (s), 128.26 (s), 127.36 (s), 127.10 (s), 126.81 (s), 126.19 (s), 124.83 (s), 121.89 (s), 39.57 (s), 29.70 (s), 22.67 (s), 21.91 (s).
HRMS (ESI): *m/z* calcd for $C_{42}H_{36}CuN_4^+$: 659.2236 $[M]^+$; found 659.2250.
UV/Vis(CH_2Cl_2): MLCT $\lambda_{max}(\varepsilon)$= 443 nm (3987 L.cm^{-1}.mol^{-1}); fluorescence (CH_2Cl_2): λ_{ex}= 443nm; λ_{em}= 698nm.
Anal. Calcd for $C_{42}H_{36}CuF_6N_4P$.0.9 CH_2Cl_2.0.15 C_5H_{12}: C, 58.78; H, 4.47; N, 6.28. Found C, 58.56; H, 4.82; N, 6.66.

[Cu(L2)$_2$]PF$_6$ (**C2**) was synthesized in a similar manner to that of (**C1**) using the following reagents: $[Cu(ACN)_4]PF_6$ (28 mg, 0.075mmol) and L1 (47 mg, 0.15mmol). Yield: (100%, 125mg). ^{1}H NMR spectrum (300MHz, $CDCl_3$) δ= 8.60 (d, $^3J_{H,H}$= 8.4Hz, 2H), 8.47 (d, $^3J_{H,H}$= 8.7Hz, 2H), 8.07 (AB, J_{AB} = 12.6Hz, 4H), 7.99 (d, $^3J_{H,H}$= 8.7Hz, 2H), 7.87 (d, $^3J_{H,H}$= 8.1Hz, 2H), 7.14 (m, 4H), 6.65 (m, 2H), 6.32 (m, 4H), 1.24 (s, 18H). ^{13}C NMR spectrum (75MHz, $CDCl_3$) δ= 168.57 (s), 157.28 (s), 143.09 (s), 139.21 (s), 137.95 (s), 137.80 (s), 128.85 (s), 128.56 (s), 128.38 (s), 127.50 (s), 126.90 (s), 126.55 (s), 125.39 (s), 124.21 (s), 38.52 (s), 30.56 (s). HRMS (ESI): *m/z* calcd for $C_{44}H_{40}CuN_4^+$: 687.2549 $[M]^+$; found 687.2541. UV/Vis (CH_2Cl_2): MLCT $\lambda_{max}(\varepsilon)$= 450 nm (3851 L.cm^{-1}.mol^{-1}); fluorescence (CH_2Cl_2): λ_{ex}= 450nm; λ_{em}= 695nm.
Anal. Calcd for $C_{44}H_{40}CuF_6N_4P$. 0.45 CH_2Cl_2: C, 61.26; H, 4.73; N, 6.43. Found: C, 61.27; H, 4.85; N, 6.50.

Computational details All calculations were performed using ADF 2019[34] package at the DFT level of theory with B3LYP functional.[35] The all-electrons slater type TZP basis set described all atoms.[36] Scalar relativistic ZORA Hamiltonian was employed.[37] Van der Waals forces were treated through the introduction of Grimme's corrections (grimme3).[38] Solvent corrections for dichloromethane were introduced through a PCM model.[39] Structures were fully optimized and the absorption spectrum was computed by mean of TD-DFT[40] on these structures with the inclusion of the Tamm-Dancoff approximation.[41] Spin-Orbit Coupling was computed by a perturbative approach. The excited states (singlet or triplet) structures were computed by the same approach. All calculations were first performed retaining the symmetry point group of the ground state. Then symmetry was broken to allow complete relaxation of the structures. For the study of Non-Covalent interactions, the complexes were reoptimized with GAUSSIAN 09 (D01)[42] package at DFT level of theory (B3LYP functional)[43] using 6-31+G** basis set[44] for all atoms (the f polarization were deleted). Again, dispersion corrections were introduced through Grimme's correction GD3 and solvent introduced through a PCM model of dichloromethane. These calculations were performed on the ground state and on the lowest triplet state of the

10.1002/chem.202001209

molecules. The natures of the encountered stationary points were characterized by a frequency analysis. The wavefunction of these complexes was then analyzed using the NCIplot package.[45]

Acknowledgements

The authors wish to thank the ANR (PERCO program n°ANR-16-CE07-0012-01) for financial support, the CEISAM (Nantes University) analysis platforms. YP is grateful to Dr. Eric Levillain from MOLTECH-Anjou for granting access to his glove box electrochemical setup. The calculations were carried out in part at the IDRIS computer centers through a grant of computer time from GENCI (A0050810629) and in part in the Strasbourg HPC.

Keywords: Copper(I) homoleptic complexes • Photochemistry • reductive quenching • DFT calculation

[1] a) N. Armaroli, G. Accorsi, F. Cardinali and A. Listorti, *Top. Curr. Chem.* **2007**, *280*, 69-115; b) M. S. Lazorski and F. N. Castellano, *Polyhedron* **2014**, *82*, 57-70; c) M. Ruthkosky, C. A. Kelly, F. N. Castellano and G. J. Meyer, *Coordination Chemistry Reviews* **1998**, *171*, 309-322.
[2] D. V. Scaltrito, D. W. Thompson, J. A. O'Callaghan and G. J. Meyer, *Coordination Chemistry Reviews* **2000**, *208*, 243-266.
[3] a) M. W. Mara, K. A. Fransted and L. X. Chen, *coordination Chemistry Reviews* **2015**, *282–283*, 2-18; b) M. Iwamura, S. Takeuchi and T. Tahara, *Accounts of Chemical Research* **2015**, *48*, 782-791.
[4] a) G. Smolentsev, A. V. Soldatov and L. X. Chen, *The Journal of Physical Chemistry A* **2008**, *112*, 5363-5367; b) D. R. McMillin, J. R. Kirchhoff and K. V. Goodwin, *Coordination Chemistry Reviews* **1985**, *64*, 83-92.
[5] a) O. Green, B. A. Gandhi and J. N. Burstyn, *Inorganic Chemistry* **2009**, *48*, 5704-5714; b) S. Garakyaraghi, P. D. Crapps, C. E. McCusker and F. N. Castellano, *Inorganic Chemistry* **2016**, *55*, 10628-10636; c) C. E. McCusker and F. N. Castellano, *Inorg. Chem.* **2013**, *52*, 8114-8120; d) M. K. Eggleston, D. R. McMillin, K. S. Koenig and A. J. Pallenberg, *Inorg. Chem.* **1997**, *36*, 172-176; e) L. Kohler, D. Hayes, J. Hong, T. J. Carter, M. L. Shelby, K. A. Fransted, L. X. Chen and K. L. Mulfort, *Dalton Transactions* **2016**; f) C. T. Cunningham, K. L. H. Cunningham, J. F. Michalec and D. R. McMillin, *Inorganic Chemistry* **1999**, *38*, 4388-4392; g) M. T. Miller, P. K. Gantzel and T. B. Karpishin, *Angewandte Chemie International Edition* **1998**, *37*, 1556-1558; h) M. T. Miller, P. K. Gantzel and T. B. Karpishin, *Inorg. chem.* **1999**, *38*, 3414-3422.
[6] R. S. Khnayzer, C. E. McCusker, B. S. Olaiya and F. N. Castellano, *Journal of the American Chemical Society* **2013**, *135*, 14068-14070.
[7] N. A. Gothard, M. W. Mara, J. Huang, J. M. Szarko, B. Rolczynski, J. V. Lockard and L. X. Chen, *Journal of Physical Chemistry A* **2012**, *116*, 1984-1992.
[8] a) C. O. Dietrich-Buchecker, P. A. Marnot, J.-P. Sauvage, J. R. Kirchhoff and D. R. McMillin, *Journal of the Chemical Society, Chemical Communications* **1983**, 513-515; b) J.-M. Kern and J.-P. Sauvage, *Journal of the Chemical Society, Chemical Communications* **1987**, 546-548; c) A. K. I. Gushurst, D. R. McMillin, C. O. Dietrich-Buchecker and J. P. Sauvage, *Inorganic Chemistry* **1989**, *28*, 4070-4072.
[9] a) M. T. Miller, P. K. Gantzel and T. B. Karpishin, *Inorganic Chemistry* **1998**, *37*, 2285-2290; b) A. Abbotto and N. Manfredi, *Dalton Transactions* **2011**, *40*, 12421-12438.
[10] K. L. Cunningham and D. R. McMillin, *Inorg. Chem.* **1998**, *37*, 4114-4119.
[11] K. De, J. Legros, B. Crousse, S. Chandrasekaran and D. Bonnet-Delpon, *Org. Biomol. Chem.* **2011**, *9*, 347-350.
[12] J. F. Dobson, B. E. Green, P. C. Healy, C. H. L. Kennard, C. Pakawatchai and A. H. White, *Australian Journal of Chemistry* **1984**, *37*, 649-659.
[13] M. W. Mara, N. E. Jackson, J. Huang, A. B. Stickrath, X. Zhang, N. A. Gothard, M. A. Ratner and L. X. Chen, *The Journal of Physical Chemistry B* **2013**, *117*, 1921-1931.
[14] A. K. Ichinaga, J. R. Kirchhoff, D. R. McMillin, C. O. Dietrich-Buchecker, P. A. Marnot and J. P. Sauvage, *Inorganic Chemistry* **1987**, *26*, 4290-4292.
[15] B. A. Gandhi, O. Green and J. N. Burstyn, *Inorganic Chemistry* **2007**, *46*, 3816-3825.
[16] P. Yang, X.-J. Yang and B. Wu, *European Journal of Inorganic Chemistry* **2009**, 2951-2958.
[17] a) G. F. Strouse, J. R. Schoonover, R. Duesing, S. Boyde, W. E. Jones, Jr. and T. J. Meyer, *Inorganic Chemistry* **1995**, *34*, 473-487; b) N. H. Damrauer, T. R. Boussie, M. Devenney and J. K. McCusker, *Journal of the American Chemical Society* **1997**, *119*, 8253-8268.
[18] D. Felder, J. F. Nierengarten, F. Barigelletti, B. Ventura and N. Armaroli, *Journal of the American Chemical Society* **2001**, *123*, 6291-6299.
[19] M. Meyer, A.-M. Albrecht-Gary, C. O. Dietrich-Buchecker and J.-P. Sauvage, *Inorganic Chemistry* **1999**, *38*, 2279-2287.

[20] L. X. Chen, G. Jennings, T. Liu, D. J. Gosztola, J. P. Hessler, D. V. Scaltrito and G. J. Meyer, *Journal of the American Chemical Society* **2002**, *124*, 10861-10867.
[21] a) G. Capano, U. Rothlisberger, I. Tavernelli and T. J. Penfold, *The Journal of Physical Chemistry A* **2015**, *119*, 7026-7037; b) A. Agena, S. Iuchi and M. Higashi, *Chemical Physics Letters* **2017**, *679*, 60-65.
[22] S. Brown-Xu, M. Fumanal, C. Gourlaouen, L. Gimeno, A. Quatela, C. Thobie-Gautier, E. Blart, A. Planchat, F. Riobé, C. Monnereau, L. X. Chen, C. Daniel and Y. Pellegrin, *Inorganic Chemistry* **2019**, *58*, 7730-7745.
[23] C. C. Phifer and D. R. McMillin, *Inorganic Chemistry* **1986**, *25*, 1329-1333.
[24] J. R. Kirchhoff, R. E. Gamache, M. W. Blaskie, A. A. Del Paggio, R. K. Lengel and D. R. McMillin, *Inorganic Chemistry* **1983**, *22*, 2380-2384.
[25] R. Czerwieniec, M. J. Leitl, H. H. H. Homeier and H. Yersin, *Coordination Chemistry Reviews* **2016**, *325*, 2-28.
[26] E. C. Riesgo, Y.-Z. Hu, F. Bouvier, R. P. Thummel, D. V. Scaltrito and G. J. Meyer, *Inorganic Chemistry* **2001**, *40*, 3413-3422.
[27] A. Stoïanov, C. Gourlaouen, S. Vela and C. Daniel, *The Journal of Physical Chemistry A* **2018**, *122*, 1413-1421.
[28] C. E. Atkins, S. E. Park, J. A. Blaszak and D. R. McMillin, *Inorganic Chemistry* **1984**, *23*, 569-572.
[29] E. Gumienna-Kontecka, Y. Rio, C. Bourgogne, M. Elhabiri, R. Louis, A.-M. Albrecht-Gary and J.-F. Nierengarten, *Inorganic Chemistry* **2004**, *43*, 3200-3209.
[30] K. L. Cunningham, C. R. Hecker and D. R. McMillin, *Inorganica Chimica Acta* **1996**, *242*, 143-147.
[31] J. L. Robbins, N. Edelstein, B. Spencer and J. C. Smart, *Journal of the American Chemical Society* **1982**, *104*, 1882-1893.
[32] G. Sheldrick, *Acta Crystallographica Section A* **2015**, *71*, 3-8.
[33] G. Sheldrick, *Acta Crystallographica Section C* **2015**, *71*, 3-8.
[34] G. te Velde, F. M. Bickelhaupt, E. J. Baerends, C. Fonseca Guerra, S. J. A. van Gisbergen, J. G. Snijders and T. Ziegler, *Journal of Computational Chemistry* **2001**, *22*, 931-967.
[35] P. J. Stephens, F. J. Devlin, C. F. Chabalowski and M. J. Frisch, *The Journal of Physical Chemistry* **1994**, *98*, 11623-11627.
[36] E. Van Lenthe and E. J. Baerends, *Journal of Computational Chemistry* **2003**, *24*, 1142-1156.
[37] P. H. T. Philipsen, E. van Lenthe, J. G. Snijders and E. J. Baerends, *Physical Review B* **1997**, *56*, 13556-13562.
[38] S. Grimme, J. Antony, S. Ehrlich and H. Krieg, *Journal of Chemical Physics* **2010**, *132*.
[39] A. Klamt, *The Journal of Physical Chemistry* **1995**, *99*, 2224-2235.
[40] S. J. A. van Gisbergen, J. G. Snijders and E. J. Baerends, *Computer Physics Communications* **1999**, *118*, 119-138.
[41] S. Hirata and M. Head-Gordon, *Chemical Physics Letters* **1999**, *314*, 291-299.
[42] G. W. T. M. J. Frisch, H. B. Schlegel, G. E. Scuseria, M. A. Robb, J. R. Cheeseman, G. Scalmani, V. Barone, G. A. Petersson, H. Nakatsuji, X. Li, M. Caricato, A. Marenich, J. Bloino, B. G. Janesko, R. Gomperts, B. Mennucci, H. P. Hratchian, J. V. Ortiz, A. F. Izmaylov, J. L. Sonnenberg, D. Williams-Young, F. Ding, F. Lipparini, F. Egidi, J. Goings, B. Peng, A. Petrone, T. Henderson, D. Ranasinghe, V. G. Zakrzewski, J. Gao, N. Rega, G. Zheng, W. Liang, M. Hada, M. Ehara, K. Toyota, R. Fukuda, J. Hasegawa, M. Ishida, T. Nakajima, Y. Honda, O. Kitao, H. Nakai, T. Vreven, K. Throssell, J. A. Montgomery, Jr., J. E. Peralta, F. Ogliaro, M. Bearpark, J. J. Heyd, E. Brothers, K. N. Kudin, V. N. Staroverov, T. Keith, R. Kobayashi, J. Normand, K. Raghavachari, A. Rendell, J. C. Burant, S. S. Iyengar, J. Tomasi, M. Cossi, J. M. Millam, M. Klene, C. Adamo, R. Cammi, J. W. Ochterski, R. L.

WILEY-VCH

Martin, K. Morokuma, O. Farkas, J. B. Foresman, and D. J. Fox in *Gaussian 09, Revision D.01*, *Vol.* (Ed. W. CT), **2016**.
[43] A. D. Becke, *J. Chem. Phys.* **1993**, *98*, 5648.
[44] G. A. Petersson, A. Bennett, T. G. Tensfeldt, M. A. Al‐Laham, W. A. Shirley and J. Mantzaris, *The Journal of Chemical Physics* **1988**, *89*, 2193-2218.
[45] a) E. R. Johnson, S. Keinan, P. Mori-Sánchez, J. Contreras-García, A. J. Cohen and W. Yang, *Journal of the American Chemical Society* **2010**, *132*, 6498-6506; b) J. Contreras-García, E. R. Johnson, S. Keinan, R. Chaudret, J.-P. Piquemal, D. N. Beratan and W. Yang, *Journal of Chemical Theory and Computation* **2011**, *7*, 625-632.

Entry for the Table of Contents (Please choose one layout)

Layout 1:

FULL PAPER

Substituting phenanthroline by one phenyl and one branched alkyl chain in α of the nitrogen atoms yields copper(I) complexes gathering the advantages of both kinds of substituents, provided that the steric bulk is finely tuned. This strategy allowed to implement a reductive quenching step with improved kinetics, while laying stress under the paramount importance of controlling the reorganization energy.

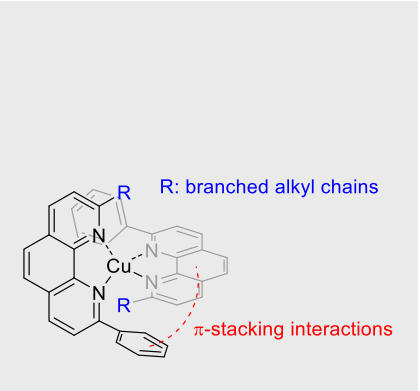

*Lea Gimeno, Errol Blart, Jean-Noel Rebilly, Marina Coupeau, Magali Allain, Thierry Roisnel, Alexis Quarré de Verneuil, Christophe Gourlaouen, Chantal Daniel and Yann Pellegrin**

Page No. – Page No.

Non symmetrical sterically challenged phenanthroline ligands and their homoleptic copper(I) complexes with improved excited state properties

10.1002/chem.202001209

WILEY-VCH